Raman response of *Stage-1* graphite intercalation compounds revisited

J.C. Chacón-Torres* and T. Pichler†
Faculty of Physics, University of Vienna, Strudlhofgasse 4, A-1090 Vienna, Austria

A.Y. Ganin and M.J. Rosseinsky
Department of Chemistry, University of Liverpool, Liverpool L69 7ZD, UK

(Dated: July 16, 2012)

We present a detailed in-situ Raman analysis of *stage-1* KC_8, CaC_6, and LiC_6 graphite intercalation compounds (GIC) to unravel their intrinsic finger print. Four main components were found between 1200 cm^{-1} and 1700 cm^{-1}, and each of them were assigned to a corresponding vibrational mode. From a detailed line shape analysis of the intrinsic Fano-lines of the G- and D-line response we precisely determine the position (ω_{ph}), line width (Γ_{ph}) and asymmetry (q) from each component. The comparison to the theoretical calculated line width and position of each component allow us to extract the electron-phonon coupling constant of these compounds. A coupling constant $\lambda_{ph} < 0.06$ was obtained. This highlights that Raman active modes alone are not sufficient to explain the superconductivity within the electron-phonon coupling mechanism in CaC_6 and KC_8.

I. INTRODUCTION

Sp^2 hybridized carbon allotropes have unique structural properties in different dimensions like graphite (3D), graphene (2D), single walled carbon nanotubes (1D), and fullerene molecules ("quasi 0D"). They have been widely studied due to their interesting electronic properties ranging from metallic, semimetallic, (zero gap) semiconducting to wide gap semiconducting and insulating [1–4]. One unique possibility to tailor their electronic properties is by intercalation of alkali and alkaline-earth ions. These intercalation compounds are particular appealing for their application in batteries and because of their superconducting phases. Superconductivity, as a result of alkali-metal intercalation, was first studied by Henning [5] in Graphite Intercalation Compounds (GIC) and further studies [6, 7]. However, until 1981, the critical temperature (T_c) in *stage-1* XC_8 GIC (X=K, Rb, and Cs) reported was low [1], not higher than 0.135 K for CsC_8, and between 0.39-0.55 K for KC_8. This is surprising since GIC are BCS superconductors based on electron phonon coupling owing an exceptionally high electron phonon coupling constant up to $\lambda = 0.45$ in the case of KC_8 and high phonon frequency of the optical modes [8]. For instance, using λ=0.45 and a phonon frequency of 1337 cm^{-1} a BCS T_c of ∼5 K would be possible in KC_8 which is much higher than the observed T_c up to 0.55 K, and this can be related to a screened Coulomb pseudopotential of $\mu^* = 0.14$, which is on the lower bound with respect to CaC_6 [9].

In 1991, the discovery of fullerene intercalation compounds, so-called fullerides, added a new family of organic superconductors of type A_3C_{60} (A=alkali-metal) [10–12]. Compared to classical superconductors, and in contrast to GIC the T_c observed in fullerides is high ranging from 18 K for K_3C_{60}, 28 K for Rb_3C_{60}, up to 39 K for Cs_3C_{60} [11–13]. Contrary to GIC, where the highest intercalation level represents the superconducting phase, for fullerides the superconducting phase is a line phase at half filling. Other stable fullerides A_1C_{60}, A_4C_{60} and A_6C_{60} are either normal metals, Mott-Hubbard insulators or charge transfer insulators [14]. Similar to GIC the superconducting coupling mechanism was described within the framework of BCS theory involving an electron phonon coupling to the intra-molecular modes of C_{60} [3]. Experimentally, most important for the coupling are the two low energy intra-molecular modes with H_g symmetry [15, 16], although theoretically the high frequency phonons have been predicted to play a significant role [17, 18].

For GIC, the observation of superconductivity of CaC_6 in 2005 with a high T_c of 11.5 K [19] triggered further research in the field and led to alternative explanations of the superconducting electron phonon coupling. For instance, Kim et al. attribute superconductivity in CaC_6 to the high-energy C modes [20]. Hinks et al. [21] report that the low-energy modes of the intercalant were responsible for superconductivity inferred from specific heat analysis, while first principle calculations predicts equal coupling to both groups of phonons [9, 22]. Therefore, the exact contribution of the different coupling phonons still remain elusive.

Raman spectroscopy became then an important tool to determine the exact contribution of each phonon, and it opened a route for revealing the coupling mechanism in superconducting fullerides and GICs. Hence, it serves as a key tool to analyze the electron phonon coupling con-

* julio.chacon@univie.ac.at; Faculty of Physics, University of Vienna, Strudlhofgasse 4, A-1090 Vienna, Austria
† http://epm.univie.ac.at

stant (λ) from a renormalization of the optical response of the intra-molecular C_{60} modes and of the graphitic G-line response. Recent Raman studies on the G-line response of different *stage-1* GIC reported the assignment of the electron phonon coupling (EPC) induced line width γ^{EPC} to the 1510 cm^{-1} mode [23–26], which has been explained by the inclusion of non adiabatic phonon calculations [24, 26]. However, the intrinsic G-line response in heavily doped graphite compounds are still elusive because of the influence of defects and laser induced deintercalation, as recently reported using a micro Raman analysis for CaC_6 [24] and for KC_8 single crystals [27].

In this contribution we report a detailed study of the D- and G-lines in KC_8, CaC_6, and LiC_6 GIC, in order to unravel their intrinsic phonon components and its relation to the electron phonon coupling constant responsible for superconductivity. From the analysis of the optical phonons observed, we assign their role in the superconductivity coupling mechanism in comparison with previous results of electron doped GIC.

II. EXPERIMENTAL, AND MEASUREMENT DETAILS

The synthesis of KC_8 was performed in-situ under high vacuum ($\sim$4x10^{-8} mbar) conditions in a quartz tube with natural graphite flake single crystals from different sources, and a potassium ingot with 99.95% purity (Aldrich) for the intercalation. Potassium was evaporated until golden crystals were obtained. This phase can be directly assigned to *stage-1* KC_8 phase from a comparison of the Raman response with previous combined Raman and XRD results [27, 28]. CaC_6, and LiC_6 were prepared in a sealed ampoule by using a procedure described elsewhere [29]. Highly oriented pyrolytic graphite (HOPG) flakes were degassed and used for lithium and calcium intercalation for 10 days under He atmosphere (ca. 0.5 atm). The ampoule was then opened in the glove box and gold colored product was extracted from the melt. Powder x-ray diffraction measurements were carried out using a Stadi-P diffractometer (CuK_a) to confirm the intercalation stage in CaC_6 and LiC_6. For the Raman analysis every GIC was kept in vacuum ($\sim$4x10^{-8} mbar) in order to avoid de-intercalation due to exposure to air. The Raman analysis, was performed with a HORIBA LabRam at room temperature, with a 568 nm wave length, and 0.25 mW of laser power. Every spectrum were acquired under the same conditions in a range from 500 cm^{-1} up to 2500 cm^{-1} and the line positions were calibrated by gauge lamps.

III. RESULTS AND DISCUSSION

In the Raman response of *stage-1* GIC eight optical vibrational modes are present [28] in the following irreducible representation:

$$\Gamma = 2A_{2u} + 2B_{2g} + 2E_{1u} + 2E_{2g}$$

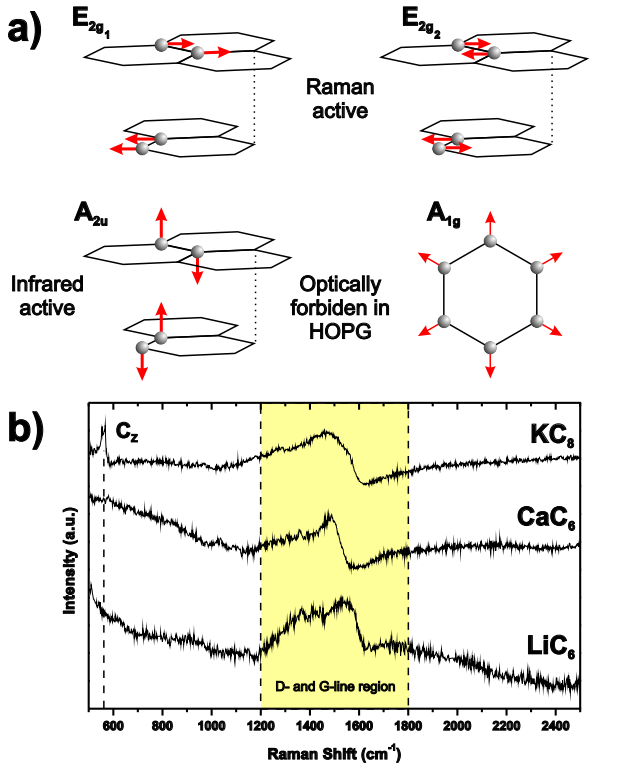

FIG. 1. a) Optical modes of graphite. b) Raman spectra from KC_8, CaC_6, and LiC_6 taken with 568 nm laser at room temperature and low laser power of 0.25 mW.

The $E_{2_{g_1}}$, and the $E_{2_{g_2}}$ vibrational modes are Raman active, and the A_{2u}, and E_{1u} belong to infra-red active modes [1, 30]. There are some other modes in graphite which are forbidden in perfect graphite and only become active in the presence of disorder like the mode with A_{1g} symmetry. In Fig. 1 a), the optical modes of graphite are depicted. Previous Raman studies in GIC have confirmed the presence of the E_{2g} mode around 1600 cm^{-1}, the A_{2u} (*c-axis* mode) around 500 cm^{-1}, and the absence of the A_{1g} [1, 28]. The *c-axis* mode has being attributed to an out-of-plane C motion in graphite [24]. This mode correspond to the **M** point of the graphene Brillouin zone, and it becomes Raman active when high intercalation levels are achieved. In agreement with the literature, we observe (as shown in in Fig. 1 b), that the *c-axis* mode is present solely in KC_8 around $\sim$560 cm^{-1}. Surprisingly and in agreement with previous studies neither in CaC_6, nor in LiC_6 this mode is observed [23, 31].

Regarding the G-line response all these previous studies reported one G-line which has a strong Fano line shape due to the coupling and the interference with the conduction electrons. Taking a closer look on the lineshape of the G-line response in Fig. 1 b), one can easily see that more than one component is present, and a detailed line shape analysis is needed in order to unravel their intrinsic response and related electron phonon coupling of these *stage-1* GIC. The line-shape analysis of the G-line is discussed in detail below.

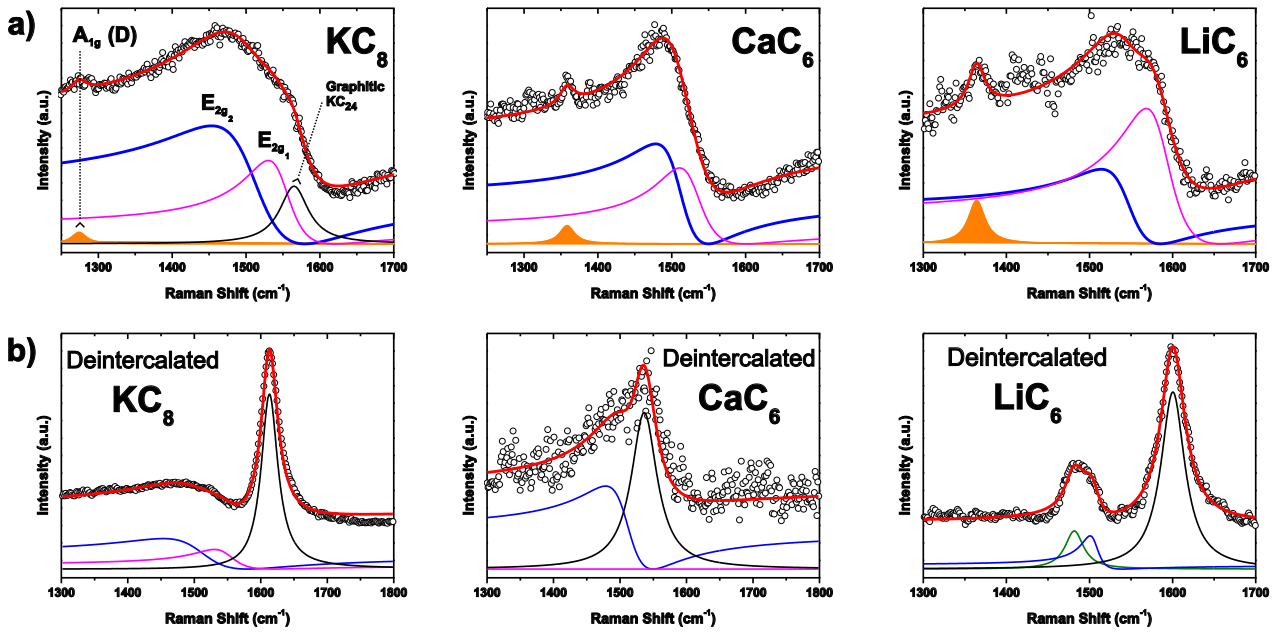

FIG. 2. D- and G-line analysis for *stage-1* GIC, and Raman response of their laser induced deintercalated phases. The four components which can be identified in the G-line shape are: $\mathbf{A}_{1g}$ mode between 1250 and 1350 cm^{-1}, $\mathbf{E}_{2g_2}$ mode ∼1510 cm^{-1}, $\mathbf{E}_{2g_1}$ mode at ∼1547 cm^{-1} , and *stage-2* G-mode ∼1560 cm^{-1}. In the upper panel **a)** we can observe that KC_8 exhibit a strong contribution from the $\mathbf{E}_{2g_2}$ with a broad Fano behavior, which is the finger print for the intrinsic line of *stage-1* compound [27]. In the lower panel **b)** we present the same crystals analyzed in the upper panel but de-intercalated. We can clearly observe the decrease of the $\mathbf{E}_{2g_2}$ mode, concomitant to a strong increase of the G-mode assigned to the XC_{24} graphitic face ∼1600 cm^{-1}.

A. Analysis of the intrinsic G-line response of *Stage-1* GIC

The structure of the intercalation stages in graphitic compounds, has been studied and it is well understood from x-ray diffraction [28]. However, the intrinsic Raman response of *stage-1* GIC is still complicated by laser induced de-intercalation from a local heating of the sample with different laser power densities [30]. In addition, other factors such as 3D intrinsic disorder of the crystal also strongly affect the Raman response in GIC. For example, a graphite single crystal doped to *stage-1* will remain polycrystalline due to a non-homogeneous intercalation. This will limit the achievable doping in these GIC [24, 32].

Hence, the previous experimental and theoretical results on the Raman response of KC_8 and CaC_6 reported in the literature are not conclusive with respect to the G-line shape and position. In different studies a wide range of different G-line positions between ∼1400 cm^{-1} and ∼1600 cm^{-1} are reported: i.e. at ∼1500 cm^{-1} [1], between 1400 cm^{-1} and 1550 cm^{-1} [28], 1534 cm^{-1} [26], 1547 cm^{-1} [30], 1420 cm^{-1} and 1582 cm^{-1} [33]. In more recent experiments for calcium GIC [24, 25], potassium doped graphene and graphite [27, 32], and later in Li-graphite [31], the strongest G-line phonon response is observed around 1510 cm^{-1} when the sample has the best quality (lowest defect content) and highest intercalation.

In Fig. 2 a) the D- to G-band region of pristine *stage-1* intercalation compounds with K, Ca, and Li is depicted and clearly shows the presence of shoulders in the response, which indicate different components. Nevertheless, in order to compare with the previous studies [26, 30, 33] we first conducted a line-shape analysis of the G-line by using a single Breit Wigner Fano (BWF) function. This yields parameters which are in good agreement to those results, and confirms that our samples have the same high quality of a true *stage-1* compound. This is further supported by the fact that the G-line assigned to *stage-2* compounds around 1600 cm^{-1} is only increased upon e.g. laser induced de-intercalation (see Fig. 2 b).

In a second step a detailed and accurate analysis of the line-shape in the D- to G-band region of these GIC was conducted using four components. The assignment of each component to the A_{1g}(D), E_{2g_2}, E_{2g_1} modes, and the G-line of the *stage-2* compound is explained in the following.

Regarding the line-shape, all components have been fitted using BWF functions of the form:

$$I(w) = I_0 \frac{(1+\frac{w-w_{ph}}{q\,\Gamma/2})^2}{1+(\frac{w-w_{ph}}{\Gamma/2})^2} + A$$

where ω_{ph} is the phonon frequency, Γ the line width or damping, **q** the asymmetry parameter and A an offset. For the first and fourth peak (D, and G), the asymmetry was $\mathbf{q}$=10^5 approaching a Lorentzian function, while the second and third (splitted G-line) have a pronounced Fano interference. In the analysis, in order to get comparable results for each GIC, the same values of Γ, and

q were used to fit each respective component. The parameters are summarized in Table I together with the calculated values from the adiabatic and non-adiabatic phonons from Ref. [26].

The first mode observed in Fig. 2 a) between 1260 and 1360 cm^{-1} has been previously attributed to particle size effects and/or the presence of disorder [34, 35]. It has been assigned to the A_{1g} vibration, which is forbidden in perfect graphite. Therefore, this mode is called D-line (intrinsic "defect mediated"), and it involves the contribution from the phonons near the K zone boundary with a Lorentzian line-shape.

The second and third modes observed are assigned to the E_{2g} graphitic mode of heavily doped graphene layers (Fig. 2 a). Both components have a pronounced asymmetry and they are well described by a BWF line-shape. We label the two modes as E_{2g_1} and E_{2g_2}. The E_{2g_1} mode is located between 1528 cm^{-1} and 1585 cm^{-1} and it is attributed to not homogeneous or incomplete intercalation in *stage-1* compounds [27]. The E_{2g_2} mode locates at 1510 cm^{-1} for KC_8 and CaC_6, and 1546 cm^{-1} for LiC_6. It has a clear and strong Fano behavior which is characteristic to the finger print of *stage-1* graphite intercalation compounds [24, 27]. When de-intercalation was induced in the samples, a decrease of these E_{2g} modes was remarkably observed (see Fig. 2 b).

The fourth mode related to the G-line of their respective *stage-2* compound is observed at 1612 cm^{-1} for KC_8, 1600 cm^{-1} for LiC_6 and at 1560 cm^{-1} for CaC_6. The surprising low frequency in the case of CaC_6 was also found in Ref. [25] and explained as a de-intercalated phase in CaC_6. As mentioned above, the increase of this fourth component is highlighted in the partly de-intercalated *stage-1* compounds in Fig. 2 b), and points towards a phase separation upon de-intercalation.

B. Analysis of the Electron-Phonon Coupling

The previous results are very important for the correct determination of the stage, and electron-phonon coupling constant λ_{ph} responsible for superconductivity within the BCS theory [24, 26, 36]. This constant is directly related to the intrinsic G-line phonon frequency, and to the adiabatic (ω_A) and non-adiabatic (ω_{NA}) phonon frequencies. Saitta et al. [26] have analyzed the EPC in many different *stage-1* GIC from a difference in the experimental phonon frequency to the calculated phonon frequency in the adiabatic and non-adiabatic limit. In order to determine the electron phonon scattering renormalized line width γ^{EPC} [24, 26] we used:

$$\frac{\gamma^{EPC}}{2} = \sqrt{(\omega_{ph} - \omega_A)(\omega_{NA} - \omega_{ph})} \qquad (1)$$

We obtain γ^{EPC} values for KC_8, CaC_6, and LiC_6 which are in very good agreement to our experimental Γ_{ph} value obtained from our BWF fit, Table II. In Fig. 3 we show the location of our γ^{EPC} with respect to the expected linear tendency to Γ_{ph} as predicted by Saitta et al. [26]. It is important to notice that some components of the G-line in KC_8, CaC_6, and LiC_6 bring a $\gamma^{EPC} = 0$, which means that they do not show the non-adiabatic effects for layered metals and therefore they do not contribute to the electron-phonon coupling constant λ_{ph}. In comparison to the experimental Γ^{exp} and γ^{EPC} from Ref. [23, 37, 38] (Fig. 3 ★), our results using the E_{2g_2} mode are in better agreement to the linear trend expected for $\Gamma \approx \gamma^{EPC}$. This confirms the importance of every optical mode in the range between the adiabatic and non-adiabatic frequency range (ω_A-ω_{NA}), and confirms that the E_{2g_2} component is the intrinsic *stage-1* vibrational mode with the strongest non-adiabatic effect on the EPC.

TABLE I. Fit parameters to the four components of the D- and G-line in the Raman spectra of KC_8, CaC_6, and LiC_6.

KC_8	$\omega_{ph}(cm^{-1})$	$\Gamma_{ph}(cm^{-1})$	q	ω_A [a]	ω_{NA} [b]
D	1274	24.3	10^5	-	-
E_{2g_2}	1510	125.6	-1.09	1223	1534
E_{2g_1}	1547	70.9	-2.02	1223	1534
G [c]	1565	47.0	10^5	-	-
CaC_6	$\omega_{ph}(cm^{-1})$	$\Gamma_{ph}(cm^{-1})$	q	ω_A [a]	ω_{NA} [b]
D	1358	24.3	10^5	-	-
E_{2g_2}	1510	71.0	-1.09	1446	1529
E_{2g_1}	1528	70.9	-2.02	1446	1529
LiC_6	$\omega_{ph}(cm^{-1})$	$\Gamma_{ph}(cm^{-1})$	q	ω_A [a]	ω_{NA} [b]
D	1364	24.3	10^5	-	-
E_{2g_2}	1546	71.0	-1.09	1362	1580
E_{2g_1}	1585	70.9	-2.02	1362	1580

[a] Calculated Adiabatic E_{2g} phonon frequencies Ref. [26] in cm^{-1}.
[b] Calculated Non-adiabatic E_{2g} phonon frequencies Ref. [26] in cm^{-1}.
[c] G-line contribution from KC_{24} *stage-2* compound.

We now turn to a detailed analysis of the EPC constant λ_{ph}. Different values have been already reported and used to calculate the critical temperature of KC_8, CaC_6, and LiC_6 with values around 5 K, 11.5 K, and 0.9 K, respectively, in agreement with some experimental and theoretical studies [8, 40]. In order to extract λ_{ph} from the phonon line-width (Γ) and position (ω_{ph}) from our Raman data we used [41]:

$$\lambda_{\Gamma,K} = \frac{A_{uc}\, F^2_{\Gamma,K}}{2\, M\, \omega_{\Gamma,K}\, v_F^2} \qquad (2)$$

where the electron-phonon coupling strength is given by D_{exp} :

$$\Delta\Gamma_G = \frac{A_{uc}\, D^2_{exp}}{8\, M\, v_F^2} \qquad (3)$$

and A_{uc} is defined as the area of the graphene unit cell, M is the carbon atom mass, v_F is the Fermi velocity, $\Delta\Gamma_G$ is the Landau damping phonon decay rate given by

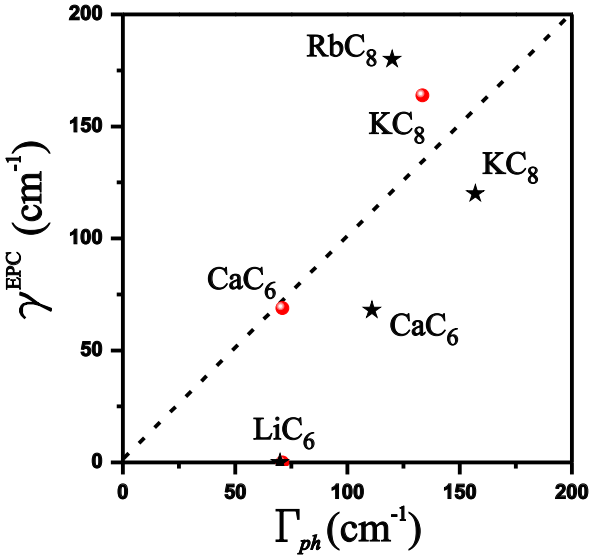

FIG. 3. Calculated γ^{EPC} (Eq. 1) for different GIC as function of their width Γ_{ph}. Black stars (★) correspond to experimental values from Ref. [23, 37, 38]. The dashed line represents the approximation of $\Gamma_{ph} \approx \gamma^{EPC}$. The red dots show our calculated EPC, which are in better agreement to the expected approximation to the Γ_{ph} values.

$\Delta\Gamma_G = \Gamma_{ph} - \Gamma_{Graphite}$, and $F^2_{\Gamma,K}$ has dimensionality of a force taking in consideration the lattice displacement along the corresponding optical phonon mode. By using Eq. 2 and the definition of $F^2_\Gamma = 4\langle D^2_\Gamma\rangle_F$, and $F^2_K = 2\langle D^2_K\rangle_F$ from Ref. [39, 41] we calculate the values for $\lambda_{\Gamma,K}$ for each phonon in the Γ-K branch observed in the G-line region as summarized in the right column of Table II. $\langle D^2_{\Gamma,K}\rangle_F$ were taken from the DFT$_{GGA}$ calculations in Graphite [39] as they are closer to our electron-phonon coupling strength (D_{exp}).

By using the averaged electron-phonon coupling constant $\lambda_{ph} = \lambda_\Gamma + \lambda_K$, and the position ω_{ph} from the strongest optical mode in KC_8, CaC_6, and LiC_6 one can estimate the critical temperature T_c using McMillan's formula [42]. Taking our ω_{ph} values converted in to phonon temperature Θ, $\mu^* \approx 0.14$ from [43], and λ_{ph} from the Raman analysis, we obtain $\lambda_{ph} < 0.06$ values, which are too low to explain superconductivity within EPC mechanism using these high-frequency Raman active modes.

However, this is not a general behavior in intercalation compounds. Electron-phonon studies in alkali-intercalated fullerenes showed the possibility to attribute the strongest λ_{ph} contribution for superconductivity to the Hg(1) mode in A_3C_{60} fullerides [15, 16]. More over, in agreement to the analysis reported by Yao et al. in Ref. [16] our D_{exp} presented the same trend as the one observed in fullerides intercalation compounds. Therefore, we can confirm that the larger the value of $1/\mathbf{q}$, the weaker the coupling strength D_{exp} in GIC and fullerides.

On the other hand, in comparison to the EPC constant

TABLE II. Electron-phonon coupling parameters from the G-line Raman analysis. The values of ω_{ph}, Γ_{ph}, γ^{EPC} are in cm^{-1} and they were extracted from the BWF analysis of the Raman spectrum. D_{exp} is the electron-phonon coupling strength from Eq. 3 in (eV/Å).

KC_8	ω_{ph}	Γ_{ph}	γ^{EPC}	γ^{EPC}[a]	D_{exp}	OB[b]	$\lambda_{K,\Gamma}$[c]
D	1274	24.3	230	-	14	K	0.024
E_{2g_2}	1510	125.6	163	157	51	Γ	0.020
E_{2g_1}	1547	70.9	0	-	36	Γ	-
λ_{ph}							0.044
CaC_6	ω_{ph}	Γ_{ph}	γ^{EPC}	γ^{EPC}[a]	D_{exp}	OB[b]	$\lambda_{K,\Gamma}$[c]
D	1358	24.3	0	-	14	K	0.022
E_{2g_2}	1510	71.0	68	68	36	Γ	0.020
E_{2g_1}	1525	70.9	34	36	36	Γ	0.019
λ_{ph}							0.061
LiC_6	ω_{ph}	Γ_{ph}	γ^{EPC}	γ^{EPC}[a]	D_{exp}	OB[b]	$\lambda_{K,\Gamma}$[c]
D	1364	24.3	43	-	14	K	0.022
E_{2g_2}	1546	71.0	157	-	36	Γ	0.019
E_{2g_1}	1585	70.9	0	0	36	Γ	-
λ_{ph}							0.041

[a] Calculated phonon full line width at half maximum due to phonon decay in dressed electron-hole pairs γ^{EPC}_σ Ref. [26].
[b] Optical branch assignment based in [8, 39].
[c] Electron-phonon coupling constant from Eq. 2

λ_{ARPES} reported using an analysis of the self energy results in ARPES [8, 44], our λ_{ph} values are about a factor of 10-15 lower. Since, in the case of CaC_6 superconductivity was confirmed at T_c=11.5 K, only the λ_{ARPES} [44] would be sufficient to explain this high superconducting transition temperature. Hence, the low λ_{ph} proves that optical modes from the G-line in *stage-1* GIC are not sufficient to explain T_c in the electron-phonon driven superconducting coupling mechanism and additional not optically active modes might play an important role.

IV. CONCLUSIONS

We have performed a detailed in-situ Raman study of the most common GIC (KC_8, CaC_6, and LiC_6). We identify four main peaks in the D- to G-band region, and all these Raman responses match the spread of different line shapes reported in the literatures so far. From an evaluation of the fine structure in the G-line response we assign each peak to their corresponding vibrational mode and phonon branch.

We found the strongest Fano behavior of the G-line at 1510 cm^{-1} in KC_8 and CaC_6, not like in LiC_6, which highlights the importance of this mode to the superconductivity coupling mechanism within the BSC theory, and confirms the importance of this E_{2g_2} mode to non-adiabatic effects. By using this mode, we obtain a very good agreement to the theoretical predicted line-width $\gamma^{EPC} \simeq \Gamma_{ph}$ especially for CaC_6.

Finally, we find a very small EPC $\lambda_{ph} < 0.06$ which is much too low to explain the high T_c in this graphite

intercalated compounds. This points out that, other phonons including acoustic modes and other electronic states might play an important role in explaining the superconducting pairing in GIC.

ACKNOWLEDGMENTS

We acknowledge for the financial support of the project FWF-I377-N16, the OEAD AMADEUS PROGRAM financing, and the comments from Dr. Hidetsugu Shiozawa and Dr. Christian Kramberger. AG and MJR thank EPSRC for funding.

[1] M. S. Dresselhaus and G. Dresselhaus, Advances In Physics **30**, 139 (1981)
[2] A. Jorio, G. Dresselhaus, and M. S. Dresselhaus, Carbon Nanotubes. Advanced Topics in the Synthesis, Structure, Properties and Applications(2008)
[3] O. Gunnarsson, Reviews of Modern Physics **69**, 575 (1997)
[4] A. H. Castro Neto, F. Guinea, N. M. R. Peres, K. S. Novoselov, and A. K. Geim, Reviews of Modern Physics **81**, 109 (2009)
[5] G. Hennig and L. Meyer, Physical Review **87**, 439 (1952)
[6] N. B. Hannay, T. H. Geballe, B. T. Matthias, K. Andres, P. Schmidt, and D. Macnair, Physical Review Letters **14**, 225 (1965)
[7] M. Kobayashi and I. Tsujikawa, Journal of the Physical Society of Japan **46**, 1945 (1979)
[8] A. Gruneis, C. Attaccalite, A. Rubio, D. V. Vyalikh, S. L. Molodtsov, J. Fink, R. Follath, W. Eberhardt, B. Buchner, and T. Pichler, Physical Review B **79**, 205106 (2009)
[9] M. Calandra and F. Mauri, Physical Review Letters **95**, 237002 (2005)
[10] R. M. Fleming, A. P. Ramirez, M. J. Rosseinsky, D. W. Murphy, R. C. Haddon, S. M. Zahurak, and A. V. Makhija, Nature **352**, 787 (1991)
[11] A. F. Hebard, M. J. Rosseinsky, R. C. Haddon, D. W. Murphy, S. H. Glarum, T. T. M. Palstra, A. P. Ramirez, and A. R. Kortan, Nature **350**, 600 (1991)
[12] M. J. Rosseinsky, A. P. Ramirez, S. H. Glarum, D. W. Murphy, R. C. Haddon, A. F. Hebard, T. T. M. Palstra, A. R. Kortan, S. M. Zahurak, and A. V. Makhija, Physical Review Letters **66**, 2830 (1991)
[13] A. Y. Ganin, Y. Takabayashi, Y. Z. Khimyak, S. Margadonna, A. Tamai, M. J. Rosseinsky, and K. Prassides, Nature Materials **7**, 367 (2008)
[14] M. Capone, M. Fabrizio, C. Castellani, and E. Tosatti, Reviews of Modern Physics **81**, 943 (2009)
[15] J. Winter and H. Kuzmany, Physical Review B **53**, 655 (1996)
[16] M. Yao, V. Pischedda, and A. San Miguel, Journal of Physics-Condensed Matter **23**, 115701 (2011)
[17] C. M. Varma, J. Zaanen, and K. Raghavachari, Science **254**, 989 (1991)
[18] M. Schlüter, M. Lannoo, M. Needels, G. A. Baraff, and D. Tomanek, Journal of Physics and Chemistry of Solids **53**, 1473 (1992)
[19] T. E. Weller, M. Ellerby, S. S. Saxena, R. P. Smith, and N. T. Skipper, Nature Physics **1**, 39 (2005)
[20] J. S. Kim, R. K. Kremer, L. Boeri, and F. S. Razavi, Physical Review Letters **96**, 217002 (2006)
[21] D. G. Hinks, D. Rosenmann, H. Claus, M. S. Bailey, and J. D. Jorgensen, Physical Review B **75**, 014509 (2007)
[22] I. I. Mazin, L. Boeri, O. V. Dolgov, A. A. Golubov, G. B. Bachelet, M. Giantomassi, and O. K. Andersen, Physica C - Superconductivity and its Applications **460**, 116 (2007)
[23] J. Hlinka, I. Gregora, J. Pokorny, C. Herold, N. Emery, J. F. Mareche, and P. Lagrange, Physical Review B **76**, 144512 (2007)
[24] M. P. M. Dean, C. A. Howard, S. S. Saxena, and M. Ellerby, Physical Review B **81**, 045405 (2010)
[25] A. Mialitsin, J. S. Kim, R. K. Kremer, and G. Blumberg, Physical Review B **79**, 064503 (2009)
[26] A. M. Saitta, M. Lazzeri, M. Calandra, and F. Mauri, Physical Review Letters **100**, 226401 (2008)
[27] J. C. Chacón-Torres and T. Pichler, Physica Status Solidi b **248**, 2744 (2011)
[28] S. A. Solin and N. Caswell, Journal of Raman Spectroscopy **10**, 129 (1981)
[29] N. Emery, C. Herold, M. d'Astuto, V. Garcia, C. Bellin, J. F. Mareche, P. Lagrange, and G. Loupias, Physical Review Letters **95**, 087003 (2005)
[30] R. J. Nemanich, S. A. Solin, and D. Guerard, Physical Review B **16**, 2965 (1977)
[31] G. L. Doll, P. C. Eklund, and J. E. Fischer, Physical Review B **36**, 4940 (1987)
[32] C. A. Howard, M. P. M. Dean, and F. Withers, Physical Review B **84**, 241404 (2011)
[33] P. C. Eklund and K. R. Subbaswamy, Physical Review B **20**, 5157 (1979)
[34] F. Tuinstra and J. L. Koenig, Journal of Chemical Physics **53**, 1126 (1970)
[35] A. C. Ferrari and J. Robertson, Physical Review B **61**, 14095 (2000)
[36] L. Pietronero and S. Strässler, Europhysics Letters **18**, 627 (1992)
[37] D. Guerard and A. Herold, Carbon **13**, 337 (1975)
[38] G. L. Doll, M. H. Yang, and P. C. Eklund, Physical Review B **35**, 9790 (1987)
[39] M. Lazzeri, C. Attaccalite, L. Wirtz, and F. Mauri, Physical Review B **78**, 081406 (2008)
[40] G. Profeta, M. Calandra, and F. Mauri, Nature Physics **8**, 1 (2012)
[41] D. M. Basko, S. Piscanec, and A. C. Ferrari, Physical Review B **80**, 165413 (2009)
[42] M. Schlüter, M. Lannoo, M. Needels, G. A. Baraff, and D. Tomanek, Physical Review Letters **68**, 526 (1992)
[43] W. L. McMillan, Physical Review **167**, 331 (1968)
[44] T. Valla and Z. Pan, *Physics and Applications of Graphene* (InTech, 2011)